TECHNICAL REPORT No. 4

to

THE OFFICE OF NAVAL RESEARCH

Contract NONR 609(43)

X-RAY DIFFRACTION STUDY OF DEFORMATION BY FILING IN BCC REFRACTORY METALS

by

E.N. Aqua and C.N.J. Wagner

Hammond Metallurgical Laboratory
Yale University
New Haven, Conn.

March, 1963

X-Ray Diffraction Study of Deformation by Filing in BCC Refractory Metals

by

E.N. Aqua and C.N.J. Wagner

Hammond Metallurgical Laboratory
Yale University
New Haven, Connecticut

Abstract

The bcc refractory metals, niobium, tantalum, vanadium, chromium and tungsten were cold worked by filing at room temperature. The broadening of the powder pattern peaks was studied by Fourier analyses of the line shapes. The effective particle sizes, $D_e(hk\ell)$, and root mean squared (rms) strains were measured in different crystallographic directions. Anisotropic values of particle sizes observed in tantalum and niobium were an indication of faulting in these metals. The degree of anisotropy of particle sizes was much smaller in vanadium; tungsten and chromium showed isotropic particle sizes.

The ratio of rms strains may be calculated from the directional variation of Young's modulus. The absolute magnitude of rms strains was also computed for isotropic bcc metals without faulting.

The amount of faulting is observed to increase with the degree of elastic anisotropy of the bcc metals of the group Vb. Metals of group VIb show no x-ray diffraction evidence of faulting.

Introduction

The broadening of x-ray powder pattern peaks of metals by cold working is evidence of microstructural changes. Analysis of the line shapes has revealed that the broadening may be separated into two factors. The first term, a size factor, is independent of the order of the reflection. It is a consequence of the small coherently diffracting domains within the crystal and/or stacking faults in the lattice. The second factor, a distortion term, contains all broadening which is dependent upon the order of reflection. The state of internal microstrains introduced by cold working is described by this distortion factor. Because faulting in the lattice makes a large contribution to the size factor, an understanding of its basic features is reviewed.

Stacking faults on the (hkℓ) planes of cubic crystals will result from a mistake in the stacking sequence of the layers of atoms in the $\langle hk\ell \rangle$ direction, parallel to the (hkℓ) plane.

The normal ABCABC stacking arrangement of (111) planes in fcc metals with its counterpart, the twinned sequence, CBACBA are described many times in the literature.[1-4] For the study of faulting in bcc metals, the crystal is thought to be composed of layers of atoms parallel to $\{112\}$ planes. The basic bcc unit cell contains six atom layers, designated ABCDEF, such that normal stacking is represented by ABCDEFABCDEF..., etc. The twinned image is given FEDCBAF..., whereas a stacking fault may be created by the insertion of an atomic plane to form ABCDCDEFA... In the hard sphere model, a small expansion of the layer spacing would be required to accommodate a layer directly above its neighbor. Although the actual insertion of planes does not occur, the stacking fault is created as a

result of a dislocation dissociation reaction. For dislocations lying on (112) planes with a Burger's vector in the [111] direction, a reaction of the type

$$\frac{1}{2}a[111] \longrightarrow \frac{1}{3}a[112] + \frac{1}{6}a[11\bar{1}]$$

produces a sessile dislocation array, as the $\frac{1}{3}a[112]$ partial dislocation is the boundary of the faulted area.[5]

The faults described above are a special type of layer faults in which the relative displacement of the faulted layer is parallel to the plane of the layer. When a change in the interplanar spacing occurs, the result is called a spacing fault.[6] The layer fault may be understood to imply a combination of both stacking faults and spacing faults.

The interpretation of line broadening in terms of faulting has been reviewed by Warren.[3] Deformation stacking faults and twin faults both contribute to the line broadening as a term in the size factor. Twin faulting is further characterized by the asymmetry of the broadened peaks. According to the faulting theory, when the net broadening, i.e., the broadening corrected for the distortion term and instrumental broadening is attributed only to the presence of stacking faults, the ratio of the effective particle sizes i.e. measured in the $\langle h_1 k_1 \ell_1 \rangle$ and $\langle h_2 k_2 \ell_2 \rangle$ directions will be a constant, e.g.

$$D_e(111):D_e(100) = 2.30:1.00 \qquad (1)$$

for faulting on (111) planes in an fcc lattice. When other phenomena e.g. coherent domains contribute to the particle size broadening, the ratio decreases, approaching 1:1 in the limiting case of isotropic domain

size. Stacking faults in fcc metals also cause a shift in the position of powder pattern peaks.

Layer faults in bcc metals have been treated for faulting on (211) planes,[6] and on (310) planes.[6] The particle size broadening, in bcc metal powder pat'ern peaks, produced by faulting alone gives rise to the follow- ratio of effective particle sizes:

$$D_e(110) : D_e(100) : D_e(112) = 2.83 : 1.00 : 1.63 \qquad (2)$$

for faulting on (112) planes. Displacement of peak position is postulated for layer faults on (211) planes with non-zero spacing faults, i.e., changes in interplanar spacing as well as in the stacking sequence. Though stacking faults in bcc metals produce peak shifts for some individual components of the (hkℓ) reflection, when an average is taken over all components, the net shift is zero for all powder pattern reflections. Hence, it is the presence of a spacing fault which produced the observed peak shifts.

Previous investigations on thoriated tungsten[8] showed that the effective particle sizes were crystallographically isotropic. The domain size in tungsten $\bar{D}$ = 200Å is thought to be a measure of the distance between dislocations in a random arrangement in the crystal. A further study on molybdenum filings recorded no evidence for faulting on (211) as a result of cold work.[9] The observed isotropic domain size $\bar{D}$ = 260Å is similar to that of tungsten. The strains are noted to be inversely proportional to the directional variation of Young's modulus.

Broadening in β-brass powder patterns indicates an anisotropic particle size. The measured ratio $D_e(110) : D_e(100)$ = 2.25:1 cannot be

understood in terms of distances between dislocations alone, but faulting on (211) planes must make an important contribution to the particle size broadening.[7] The domains in tantalum,[10] and in a tantalum -0.63 niobium alloy[11] are also anisotropic, though of a smaller ratio $D_e(110):D_e(100)$ = 1.7:1 than in β-brass. This data also suggests the presence of faulting in tantalum. A large anisotropy of effective particle size is observed in α-iron[12] $D_e(110):D_e(100)$ = 2.00:1.00. Peak shifts were observed in niobium filings, suggesting the presence of layer faults, but not in tantalum filings.[6] If one interprets the line broadening for tantalum in terms of faulting, then the absence of peak shifts indicates that there will be no spacing faults, but only stacking faults.

Evidence for faulting is also found in the intermediate phase β-AlNi.[13] This alloy, which forms a superlattice structure, exhibits an anisotropic broadening of the fundamental lines, i.e., $D_e(110):D_e(100)$ = 2.6:1.0. Two independent investigations[14,15] on Fe-Ni martensites observed that cold working of this bcc phase produces anisotropic broadening. One value of the ratio of effective particle sizes approaches that of the theoretical ratio, $D_e(110):D_e(100):D_e(112)$ = 2.8 ~ 3.0:1.0:1.5; from the other study,[15] the ratio is slightly less anisotropic, i.e., 2.3:1.0:1.3 respectively. Deformed Fe-16Cr-12Ni[15] shows similar anisotropic particle sizes.

Anisotropic broadening may be produced in pure iron by cathodic charging with hydrogen.[16] The experimental ratios of 2.12:1.00:1.53 may also be measured for pure iron deformed 5% in tension.

The purpose of this research is to continue the investigation of the sources of line broadening in the other Group VB and VIB metals.

From the previous studies (on both fcc and bcc metals) of faulting, it appears that the metals exhibiting isotropic effective particle size are also elastically isotropic, or show only small deviation from the true isotropic state. On the other hand, metals with a large degree of elastic anisotropy contain anisotropic domains. If the methods of analysis used previously to separate the distortion and size factors are the correct ones, then the anisotropy of particle sizes is a real characteristic of the metal.

A measure of anisotropy A is defined as $A = 2S_{44}/(S_{11}-S_{12})$ where S_{ij} are the elastic compliances. True isotropic metals, e.g., tungsten, have an A = 1.0. If the same anisotropy of particle size exists for metal with A values greater and less than unity, then the interpretation of the particle size in terms of faulting appears to be correct.

Experimental Procedure

Cold working of the refractory metals (niobium, tantalum, vanadium, tungsten and chromium) was achieved by hand filing at room temperature. Steel contamination was removed by magnetic separation. The filings, screened through 150 mesh, were encapsulated in fused quartz under a vacuum. Chromium and vanadium powders were each annealed at 1000 $\pm$10°C for 1 hr., niobium powders at 1100°C for 3 hours, and tantalum powder at 1100°C for 5 hours. Debye-Scherrer photograms indicated complete recrystallization for all the respective heat treatments.

Annealed filings were screened further to -325 mesh, and then all filings were compacted into briquets using Duco cement as a binder, and flattened with a glassplate.

THIS
PAGE
IS
MISSING
IN
ORIGINAL
DOCUMENT

standard for all methods used. The measured value of the lattice parameter 3.1651 Å, using CuKα, is in good agreement with the published value.

To accurately determine the background level of the cold worked peaks, the comparison method, after Sato,[14] was used. This approach entails the measurement of diffracted intensity for both cold worked and annealed powders over the entire diffractometer range. The diffracted intensity from the same metal varies with pressure of densification, the amount of binder, and the smoothness of the compacted surface of the powder. Nevertheless, the ratio of annealed powder intensity to cold worked powder intensity will be a constant, very near to unity, for all values of 2θ, whenever the intensity is that of the true background. The achievement of this uniform ratio was used as an indication of the measurement of the true background level for cold worked peaks.

Experimental Results:

Peak Position Measurements

Precision lattice parameter measurements were made from both cold worked and annealed metals. Experimental errors are anticipated to result from (1) temperature fluctuation; (2) displacement of the specimen surface from tangency to the focusing circle; and, (3) macroscopic unevenness of the specimen surface.[18]

Temperature differences of $\pm 2^{\circ}C$ during the measurement of a given series of peak positions would cause a maximum error of < 0.0001 Å in the correct lattice parameter, due to the thermal expansion (averaged for the refractory metals). Examination of the diffractometer geometry indicates that the function $f(\theta) = \frac{\cos^2\theta}{\sin\theta}$ will compensate for the displacement error of the sample from the diffractometer axis.

Figure 1 shows the plot of the lattice parameters $a_{hk\ell}$ as a function of $f(\theta)$ for the tungsten standard and chromium samples. A positive slope of the $a_{hk\ell}$-VS-$f(\theta)$ curve indicates the displacement of the sample surface behind (or below) the focusing circle. The true lattice parameter, a_o, is that value of $a_{hk\ell}$ extrapolated to $\frac{\cos^2\theta}{\sin\theta} = 0$.

There is no evidence (see figure 2) that peak shifts occur in any regular manner for niobium, tungsten, tantalum, vanadium or chromium after cold working as is predicted by the spacing fault theory for bcc metals. There are no measurable changes in lattice parameter for tungsten or chromium upon cold working.

Peak Broadening

The Fourier coefficients for chromium are shown in Figure 3, plotted as a function of the distance L normal to the reflecting planes (hkℓ). This distance $L = n d_{hk\ell}$, is the product of the harmonic number n, and the interplanar distance $d_{hk\ell}$ of the reflecting lattice planes. To separate the effect of strain and particle size on the broadening, the Warren-Averbach method is followed.[3] The distortion broadening is dependent upon the order of the reflection, whereas the particle size coefficients are independent variables. The coefficient may be written

$$\ln A_L = \ln A_L^P + \ln A_L^D(h_o) \qquad (3)$$

where A_L are the measured coefficients

A_L^P are the particle size coefficients

A_L^D are the strain coefficients, dependent upon

$h_o = (h^2+k^2+\ell^2)^{1/2}$, the order of reflection.

For small values of n and h_o, the distortion coefficient A_L^D which equals $\langle \cos 2\pi \frac{h_o}{a} L \epsilon_L \rangle$ may be expanded, and equation (1) is then written in terms of a mean squared strain $\langle \epsilon_L^2 \rangle$:

$$\ln A_L = \ln A_L^P - \frac{2\pi^2 L^2}{a^2} \langle \epsilon_L^2 \rangle h_o^2 \qquad (4)$$

where a is the lattice parameter and $\langle \epsilon_L^2 \rangle$ is the component of the mean square strain normal to the reflecting planes, and averaged over the length L and over all of the sample.

In Figure 4, the plot of $\ln A_L$ as a function of h_o^2 is drawn for chromium from the data supplied in Figure 3. The intercept value of $\ln A_L$ at $h_o^2 = 0$ gives the particle size coefficient A_L^P, and the slope is proportional to the root mean squared (rms) strain components $\langle \epsilon_L^2 \rangle^{1/2}$. When the particle size coefficients obtained from the (hkℓ) reflections are plotted as a function of L, the intercept on L of the initial slope is termed the effective particle size, $D_e(hk\ell)$ normal to the (hkℓ) planes, i.e. in the $\langle hk\ell \rangle$ direction. Figures 5 through 8 show the corresponding curves for niobium, tantalum, tungsten, and vanadium. From these curves, the values of $D_e(hk\ell)$ are calculated, and are presented in Table 1.

Discussion

From the curves in Figure 9, it is seen that the measured particle size for tungsten is isotropic, $D_e = 220\text{Å}$. This portion of the experiment was a repetition of the study by McKeehan and Warren,[8] who also found an isotropic particle size of the same magnitude (200Å).

Chromium also possesses an isotropic particle size, but slightly larger than that of tungsten, i.e., $D_e = 285\text{Å}$. These domains are the

same size as those observed in molybdenum (260Å).[9] Due to the brittle nature of the chromium, the degree of deformation in each batch of filings varied. This was evidenced by the fact that the $D_e(hk\ell)$ change from one sample to another, within the range from 250 - 300Å. However, for each individual sample, the observed D_e was in all cases, isotropic.

Reexamination of Figure 3 for chromium shows that the A_L^P follow a straight line dependence upon L, from L = 20Å to L = 100Å. Below L = 20Å, the A_L^P curve exhibits the well-known hook effect, described many times in earlier studies.[3] The importance of this constant slope is understood in terms of the distribution of particle sizes. A distribution function p(L) is introduced, and the Fourier coefficients are written in terms of this function. The second derivative of A_L^P with respect to L is written

$$\frac{d^2A_L^P}{dL^2} = -\frac{1}{\langle D\rangle}p^{(L)} \qquad (5)$$

where $\langle D\rangle$ is the particle size, and

$p^{(L)}$ is the distribution function of crystallite sizes

L cells long in the $hk\ell$ direction.

Physically the constant slope observed implies that the distribution function $p^{(L)}$ is a very narrow one. This means that there is only a small range in size of domains in chromium.

From Table 1, one sees that the values of $D_e(110)$ and $D_e(100)$ for tantalum are in good agreement with those observed in previous studies.[10,11] The large anisotropy of the ratio $D_e(110):D_e(100) = 1.62$ will be interpreted as evidence for faulting in tantalum.

The effective particle sizes in niobium are slightly less anisotropic than those in tantalum. The particle sizes in the ⟨110⟩, ⟨100⟩ and ⟨112⟩ directions are 215Å, 140Å, and 120Å respectively. The value of $D_e(112)$ = 120Å is somewhat lower than is anticipated by the faulting theory. This is attributed to the errors involved in accurately determining the background level on either side of the (422) peak measured with Mo radiation. If the tails of the broadened peak are cut too short during the analysis, the zeroth coefficient will be too small and consequently all $A_L(422)$ will be too large.

Measurement of the true background for the niobium (400) was achieved without difficulty, as the (400) was not broadened as much as the (220) peak. For tantalum, the opposite is true, and extreme care must be taken in selecting the correct (400) background level. In each case, the proper measurement of (400) gives anisotropic particles for tantalum and niobium indicating the presence of faulting.

The effective particle sizes may be rewritten such that they are interpretable in terms of the actual size of domains in the crystal, and stacking faults.[15]

$$\frac{1}{D_{e(110)}} = \frac{0.48}{D^*} + \frac{0.79}{T} + \frac{(1.5\alpha+\beta)}{a}\,\frac{2}{3\sqrt{2}} \qquad (6a)$$

$$\frac{1}{D_{e(100)}} = \frac{0.54}{D^*} + \frac{0.80}{T} + \frac{(1.5\alpha+\beta)}{a}\,\frac{4}{3} \qquad (6b)$$

The above equations are valid for small L, and small values of stacking fault and twin fault probabilities α and β respectively. D* is the actual size of the domains normal to the fault planes (211), and T is the dimension of the faulted region in the (211) planes, of a metal with

lattice parameter, a. Because their functional dependence on orientation is small, the first two right hand terms in 6a and 6b may be equated

$$\frac{1}{D} = \frac{0.48}{D^*} + \frac{0.79}{T} = \frac{0.54}{D^*} + \frac{0.80}{T} \qquad (7)$$

such that D now represents the average actual domain size in the crystal, independent of orientation factors. Values of D and $(1.5\alpha+\beta)$ calculated from equations (6a) and (6b) as modified by equation (7) are presented in Table II. The fault probabilities for tantalum, iron and niobium are the same, which is expected for metals with large anisotropic particle sizes. Small amounts of faulting are measured for vanadium, and none for tungsten, chromium and molybdenum.

In the limiting case when $D^* \rightarrow \infty$, the value of T represents the minimum distance between adjacent boundaries in the fault plane. The values of this minimum T, written T_{min}, as calculated for some bcc metals by Wagner, et al.[6] is related to D by the equation $T_{min} = 0.8D$, neglecting small differences due to orientations.

The root mean squared strain, calculated from the slope of the $\ln A_L$ vs. h_o^2 curves for each metal, according to equation (3), are presented in Figures 9 and 10 for all the metals. The strain decreases with increasing L, reaching an asymptotic value, characteristic of the metal and crystallographic direction. The shape of the strain distribution as a function of L is consistent with the picture of dislocation arrangement in these crystals. Due to the long range interactions of the stresses around a dislocation, the balance of positive and negative stresses will produce an asymptotic strain value, at some average distance away from the source of stress. The values of rms strains averaged over the distance L from

20A to 100A are tabulated in Table III. In addition, it is observed that the strains measured at L = 50Å are essentially equal to the corresponding average values.

The variation of strains in the different crystallographic directions may be predicted by examination of the directional variation of Young's modulus. Using the elastic compliances S_{ij}, one may compute the directional Young's modulus, $E_{hk\ell}$, from the equation

$$E^{-1}_{hk\ell} = S_{11} - 2[S_{11} - S_{12} - \tfrac{1}{2} S_{44}]\Gamma \tag{8}$$

$$\Gamma = \frac{h^2k^2 + k^2\ell^2 + \ell^2h^2}{(h^2 + k^2 + \ell^2)^2} \tag{8a}$$

The values of the compliances S_{ij}, the orientation factor Γ, and $E_{hk\ell}$ for representative directions are also given in Table 3. If the stress distribution during filing is isotropic, then the residual microstrains in the $\langle hk\ell \rangle$ direction will be inversely proportional to the directional Young's modulus, i.e., $\langle \epsilon^2 \rangle^{1/2}_{hk\ell} \propto E^{-1}_{hkl}$. In addition, the ratio of strains will be inversely proportional to the ratio of Young's modulus. From Table 3, the good agreement between calculated and measured ratios of strain is noted. Tungsten is observed isotropic, as is expected. The measured strain ratio in chromium is 1.20 whereas the calculated one is 1.22. Vanadium has an observed ratio of 1.19 against a predicted value of 1.22. The large elastic anisotropy for both niobium and tantalum are measured as predicted, although the anisotropy factors are opposite in nature. For niobium, the measured ratio is 1.43 compared to the expected 1.59 ratio. For tantalum, the measured value is 0.78 compared to the computed ratio of 0.756. The fact that the measured strain ratios

approach the high values anticipated by the isotropic stress model indicates that the stress is nearly isotropic. However, the model does not offer a method for calculating the distribution of strain as a function of L.

The isotropic stress model yields only values of the ratio of strain in the different crystallographic directions. A method for the calculation of the asymptotic strain in a given $\langle hk\ell \rangle$ direction for an isotropic metal is presented by Ryaboshapka and Tikhanov.[19] They consider the distortions surrounding dislocation arrays, after the manner of Eshelby, et al.[20] for cubic lattices. For elastically isotropic bcc crystals containing slip in the $\langle 111 \rangle$ direction on all $\{110\}$, $\{112\}$ are $\{123\}$ planes the crystallographic mean squared strain is calculated separately, for strain due to edge dislocation, and screw dislocation. For these calculations, it is assumed that the dislocations are not dissociated, such that the distance between dislocation, 2R, may be used to calculate the density of dislocations. The mean squared strain due to edge dislocations is

$$\langle \epsilon^2 \rangle_{hk\ell} = J \cdot \frac{72\nu^2 - 68\nu + 25}{144(1-\nu^2)}\left[1 + \frac{24\nu^2 - 44\nu + 19}{72\nu^2 - 68\nu + 25}\Gamma\right] \qquad (9)$$

where $J = \frac{b^2}{4\pi^2 R^2} \ln\frac{R}{r_o}$

b is the Burger's vector, 2R is the average distance between dislocations, r_o is the size of the dislocation core, and ν is the Poisson's ratio.

The mean squared strain due to pure screw dislocations is given

$$\langle \epsilon^2 \rangle_{hk\ell} = \frac{2}{9} J(1-2\Gamma) \qquad (10)$$

Application of these last two equations for tungsten for the calculation of the same strain ratios as before gives the following results. The calculated rms strain is 1.9×10^{-3}, which is the same as the asymptotic measured value. If the entire deformation were due to edge dislocations, then according to formula (11), the ratio $\frac{\langle \epsilon^2 \rangle_{110}^{1/2}}{\langle \epsilon^2 \rangle_{100}^{1/2}} = 1.01$. If it is assumed that all strains are a result of the presence of screw dislocations alone, then the difference between mean squared strains for the different directions is quite large, i.e. $\frac{\langle \epsilon^2 \rangle_{110}^{1/2}}{\langle \epsilon^2 \rangle_{100}^{1/2}} = 0.71$. Therefore, the result of this isotropic elasticity model is that the cold working of tungsten produces many more edge dislocations than screws.

In order to calculate J, the value of 2R formula (9) and (10) that is used in chosen such that $2R = \bar{D}$ measured by the broadening.

Applying this method to chromium, there is good agreement between observed and calculated strains and strain ratios. The observed strains have average values of 3.3×10^{-3} and 2.9×10^{-3} for the $\langle 110 \rangle$ and $\langle 100 \rangle$ directions, respectively, giving a ratio of 1.14. Assuming all edge dislocations, the strains are 2.14×10^{-3} and 1.96×10^{-3}, respectively, and a ratio of 1.09. This is a very good agreement between the measured and calculated values of the ratios of strains in the different crystallographic directions. However, since we assumed that only edge dislocation are present and that chromium is elastically isotropic, the absolute magnitudes of strains are not in agreement. Assuming that the screw dislocation produces all the deformation, the strains and ratios are 2.32×10^{-3}, 3.32×10^{-3}, and 0.71 respectively. The value for $\langle \epsilon^2 \rangle_{100}^{1/2}$ does

not agree at all with the observed value and reveals the limitation of this model. The strain ratio produced by screw dislocations alone will be a constant for isotropic media, for a given value of $\bar{D}$.

When one plots the strain ratios as a function of the anisotropy, we see the expected decrease in ratio, as one would calculate from the ratio of directional Young's modulus. Since these strain values approach the theoretical ones, the stresses in the filings are nearly isotropic.

Using the isotropic approximation for vanadium, the picture of deformation is more reasonable than that for tungsten and chromium. The observed strains are midway between those predicted by the edge dislocation or the screw dislocation models. This indicates an equal amount of edge and screw dislocation. In the strain calculation, the value D was equated to 2R, the average distance between dislocation. Continuing on this assumption, we can calculate the approximate dislocation density in the filed metals by the relationship

$$2R = \bar{D} = \rho^{-\frac{1}{2}} \tag{11}$$

computed values as listed in Table III.

In another series of calculations, Ryaboshapka and Tikhanov[21] study metals with elastic anisotropy. However, no provision is made in their equations for the changes in stress fields due to the dissociation of dislocations and production of faulted regions. Therefore, a calculation of the strains in metals containing stacking faults was not attempted.

Correlating the results from the particle size measurements and the strain calculations, we are led to the conclusion that the degree of faulting in bcc metals is dependent upon the relative elastic anisotropy

of the crystal lattice. The particle size ratios are plotted as a function of the anisotropy factor A, in figure 11. For a completely isotropic metal, such as tungsten $S_{11} - S_{12} = \frac{1}{2} S_{44}$, and A = 1. The metals which are isotropic or only slightly anisotropic contain isotropic particle sizes, e.g., W, Mo, Cr. The bcc metals which have high degrees of anisotropy have effective particle sizes which are definitely anisotropic. This is true for values of $A<1.0$ or $A>1.0$, e.g., niobium, tantalum, iron and β-brass. Since anisotropy of particle size is a real phenomenon, and not the result of an arbitrary separation of size and distortion factors, one is left with the need of a theory that would predict such anisotropy. Such a prediction may be made from the theory of faulting in bcc metals.

A significant amount of evidence from a variety of supplementary experimental techniques indicates that the high value of x-ray-determined fault probabilities observed in this study could be interpreted as the result of micro-twinning.

Changes in the microstructure, e.g., arrangement of dislocation and amount of twinning, as a function of deformation in bcc metals and alloys will occur if (1) the temperature of deformation is lowered, (2) the velocity of deformation is increased, or (3) an alloying element is added.[25] The ability to relieve internal stresses by cross-slip also decreases under these conditions. Viewed in this light, the large strains and high strain rates in the filing deformation could easily produce a twin mode of deformation in metals which normally do not twin at room temperature.

This change in the manner of deformation from slip to twinning has

been observed[31] and confirmed[32] for both pure α-iron and alloys of iron-silicon. Iron deforms by slip at room temperature, under the strain rates applicable by a tensile test. However large quantities of Newmann lamellae, i.e., twins, are found when the same metal is tested by impact loading. Twins also appear on fracture surfaces, and in surfaces close to the fracture path implying that the shock of fracture will cause the twins to form. When the deformation takes place at very low temperatures, the twinning mechanism operates for both α-iron[27] and silicon-iron alloy,[28] regardless of the method of load application. The addition of silicon to α-iron allows twins to form in badly distorted (prestrained) lattices, where twinning might not otherwise occur.[33] Studies now in progress, by the authors, on silicon-iron alloys (1 - 4% silicon) indicate that the faulting probability increases with percentage of silicon. If the addition of silicon acts to prevent cross-slip, then twinning would be the more favorable mode of stress relaxation.

Deformation twins about 40Å wide have been observed in the isomorphous alloy of Fe-3.17 P . These twins form after only a small strain in compression and give rise to a serrated stress-strain curve.[25] Many of the bcc metals that have been studied by the line profile analysis methods, have also been examined by supplementary experiments. Both β AlNi and β CuZn show a large anisotropy of effective particle size. In addition, the determination of the degree of long range order in these alloys shows that the disordering produced by the plastic deformation (slip, twinning, and faulting) is very small.[13] Twin faulting introduces the least disturbance to the order, as compared with other faults.[7]

Martensite platelets of Fe-20Ni-0.8C steels have been found to

contain very narrow internal twins, with an average width of 100Å, and a similar spacing between the twins.[24] Another electron microscopy investigation of Fe-30Ni alloy shows that, even with the absence of carbon, twinning occurs in the martensite plates. These twins themselves may be intensely faulted as the twin structure micrographs contains diffraction contrast within the twin.[26] If one compares the x-ray fault probabilities for these martensites with those of α-iron, one is lead to conclude that the large fault probability is a measure of the twinned martensite platelets.[14,15]

The degree of micro-twinning in niobium-vanadium alloys has been observed to be dependent upon alloying content and deformation temperature, as well as other factors. By increasing the percentage of vanadium, twinning was observed to occur under conditions where neither pure metal would twin, e.g., at 110C with deformation by rolling. In a molybdenum alloy containing 35 percent rhenium, deformation twins occur in abundance at room temperature.[30] A series of isomorphous alloys of niobium and rhenium, currently under investigation by the authors, also have been found to have a fault probability that goes through a maximum as the percentage of rhenium is increased.

References

1. M.S. Paterson, J. Appl. Phys., 23, 805 (1952).
2. C.S. Barrett, Structure of Metals, McGraw-Hill, New York (1952).
3. B.E. Warren, Progr. in Metal Phys., 8, 147 (1959).
4. W.T. Read, Jr., Dislocations in Crystals, McGraw-Hill, New York (1953).
5. A.H. Cottrell, Dislocations and Plastic Flow in Crystals, Clarendon, Oxford (1956).
6. C.N.J. Wagner, A.S. Tetelman, and H.M. Otte, J. Appl. Phys., 33, 3080 (1962).
7. O.J. Guentert and B.E. Warren, J. Appl. Phys., 29, 40 (1958).
8. M. McKeehan and B.E. Warren, J. Appl. Phys., 24, 52 (1953).
9. J. Despujols and B.E. Warren, J. Appl. Phys., 29, 195 (1958).
10. F.R.L. Schoening, Acta Met., 4, 510 (1956).
11. L.P. Moratsov and B.I. Smirnov, Fiz. Tverdogo Tela, 3, 1272 (1961).
12. C.N.J. Wagner, Arch. Eisenhüttw., 29, 489 (1958).
13. G.P. Mohanty and J.J. Wert, Acta Met., 11, 217 (1963).
14. S. Sato, Japan J. Appl. Phys., 1, 210 (1962).
15. A.J. Goldman and C.N.J. Wagner, Acta Met. (in press).
16. A.S. Tetelman, C.N.J. Wagner, and W.D. Robertson, Acta Met., 9, 205 (1961).
17. W.A. Rachinger, J. Sci. Instr., 25, 254 (1948).
18. B.D. Cullity, Elements of X-Ray Diffraction, Addison-Wesley, Reading, Mass. (1959).
19. K.P. Ryaboshapka and L.V. Tikhonov, Fiz. metal. metalloved, 11, 489 (1961).
20. J.P. Eshelby, W.T. Read and W. Shockley, Acta Met., 1, 251 (1953).
21. K.P. Ryaboshapka and L.V. Tikhonov, Fiz. metal. metalloved, 12, 1 (1961).

22. A. Taylor, X-Ray Metallography, Wiley, New York (1961).

23. D.I. Bolef, J. Appl. Phys., 32, 100 (1961).

24. P.M. Kelly and J. Nutting, J. Iron and Steel Inst., 197, 199 (1961).

25. E. Hornbogen, Trans. Am. Soc. Metals, 56, 16 (1963).

26. Z. Nishiyama and K. Shimizu, Acta Met., 9, 980 (1961).

27. A.W. Sleeswyk and J.N. Helle, Acta Met., 9, 344 (1961).

28. D. Hull, Acta Met., 9, 191 (1961).

29. D.O. Hobson and C.J. McHargue, 92nd AIME Annual Meeting, (Abstract), J. Metals, 15, 91 (1963).

30. E. Votava and A.W. Sleeswyk, Acta Met., 10, 965 (1962).

31. C.F. Tipper and A.M. Sullivan, Trans. Am. Soc. Metals, 43, 906 (1951).

32. C.F. Tipper and E.O. Hall, J. Iron and Steel Inst., 175, 9 (1953).

33. E.O. Hall, Twinning and Diffusionless Transformations in Metals, London (1954).

Table I: Directional Variation of Young's Modulus

Metal	Elastic Compliances*			Young's Modulus+			Anisotropy	Reference
	S_{11}	$-S_{12}$	S_{44}	E(110)	E(100)	E(111)	$A(S_{ij})$	
Vanadium	0.683	0.513	2.347	1.23	1.46	1.17	0.79	23
Niobium	0.660	0.233	3.50	0.95	1.51	0.75	0.51	23
Tantalum	0.686	0.258	1.212	1.93	1.46	2.17	1.6	23
Chromium	0.305	0.0495	0.990	2.67	3.27	2.51	0.71	23
Molybdenum	0.28	0.078	0.91	3.0	3.6	2.9	0.79	22
Tungsten	0.257	0.073	0.660	3.89	3.89	3.89	1.00	22
Iron	0.743	0.277	0.846	2.31	1.32	2.82	2.4	22

* 10^{12} cm ^{2}/dyne

+ 10^{12} dyne/cm^2

Table II (a): Anisotropic Particle Size Measurements

Metal	Deformation Conditions	$D_e(110)$ Å	$D_e(100)$ Å	$D_e(112)$ Å	$\frac{D_e(110)}{D_e(100)}$	$1.5\alpha+\beta$	D Å	Reference
Vanadium	Filed, RT	200	170		1.17	0.003	220	*
Tantalum 1	Filed, RT	210	130		1.62	0.011	315	*
'' 2	Filed, -183°C	170	100		1.70	0.016	275	10
'' 3	Filed, RT	210	120	130	1.75	0.014	360	11
Niobium	Filed, RT	215	140	120	1.54	0.010	305	*
Iron	Filed, RT	280	140		2.00	0.012	620	12
Fe-Ni 27	Transformed, <0°C	200	65	100	3.0	0.033		14
27	Filed, RT	170	60	90	2.8			14
'' 30	Filed, -196°C	85	35	45	2.3	0.057	350	15
β CuZn	Filed, RT	180	80		2.25	0.024	570	7
β AlNi	Filed, RT	195	75		2.6	0.027	1210	13

* This investigation

R.T. = Room Temperature

Table II (b): Isotropic Particle Size Measurements

Metal	$\langle D_e \rangle$, Å	Deformation Conditions	Reference
Chromium	285	Filing at R.T.	*
Tungsten 1	220	Filing at R.T.	*
" 2	200	Filing at R.T.	8
Molybdenum	260	Filing at R.T.	9

* This investigation

R.T. = Room Temperature

Table III: Strain Calculations

Metal	$\frac{E(100)}{E(110)}$	$\langle \epsilon^2 \rangle^{1/2}_{hk\ell}$						$\frac{\langle \epsilon^2 \rangle^{1/2}_{(110)}}{\langle \epsilon^2 \rangle^{1/2}_{(100)}}$		
		Measured		Equation 9		Equation 10		Measured	Equation 9	Equation 10
		(110)	(100)	(110)	(100)	(110)	(110)			
Vanadium	1.19	.0035	.0029	.00202	.00187	.00229	.00323	1.22	1.08	0.71
Tantalum	0.756	.0032	.0041					0.78		
Niobium	1.59	.0040	.0028					1.43		
Chromium	1.22	.0033	.0029	.00214	.00196	.00232	.00332	1.20	1.09	0.71
Tungsten	1.00	.0022	.0022	.0019	.0019	.00286	.00407	1.00	1.01	0.71

Figure 1 Precision lattice parameter measurements of annealed and cold worked tungsten and chromium filings. Intercept value at $\theta = 0$ is the true lattice parameter.

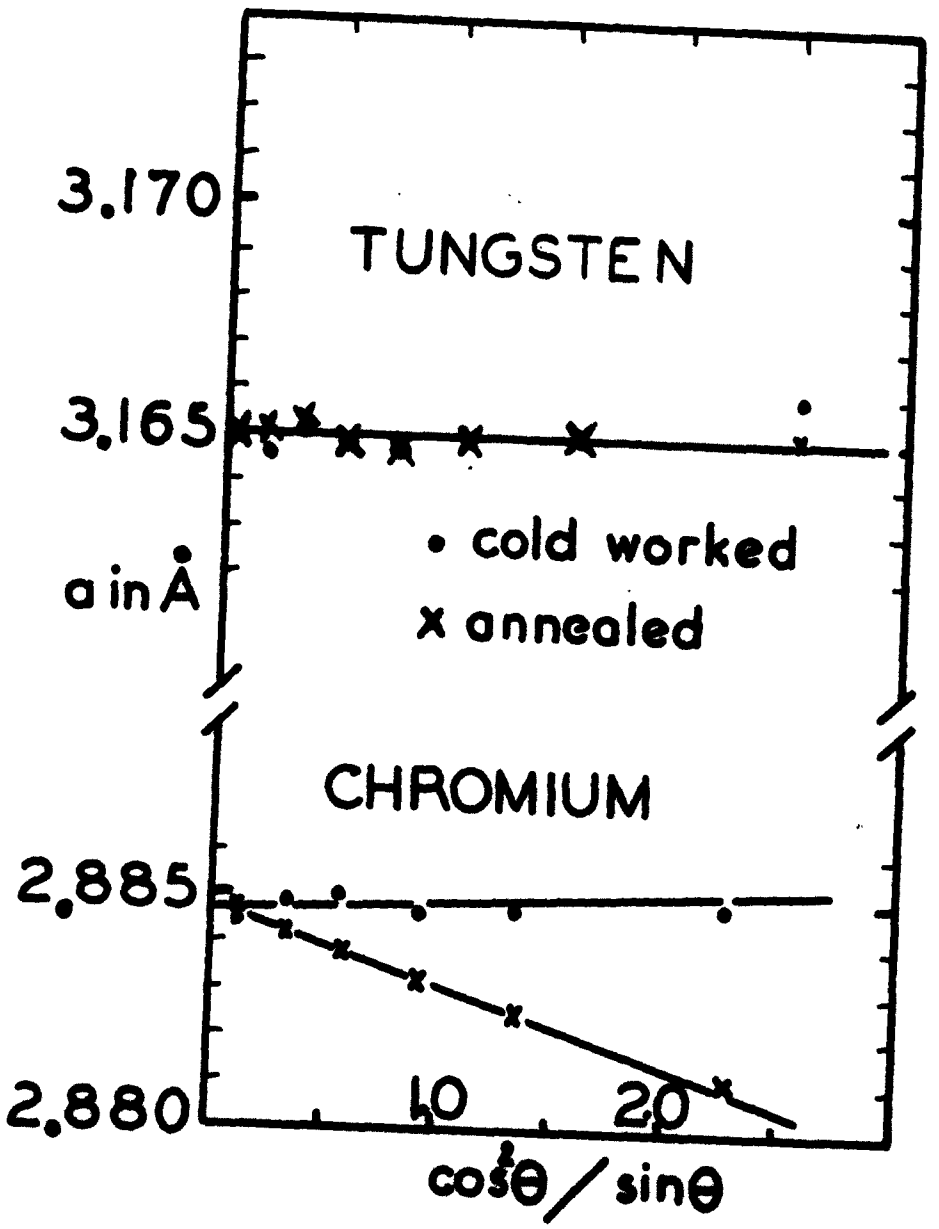
3.170
TUNGSTEN
3.165
• cold worked
a in Å
x annealed
CHROMIUM
2.885
2.880
10
20
cos²θ / sinθ

Figure 2 Precision lattice parameter measurements group V metals cold worked by filing. No systematic peak shift is observed.

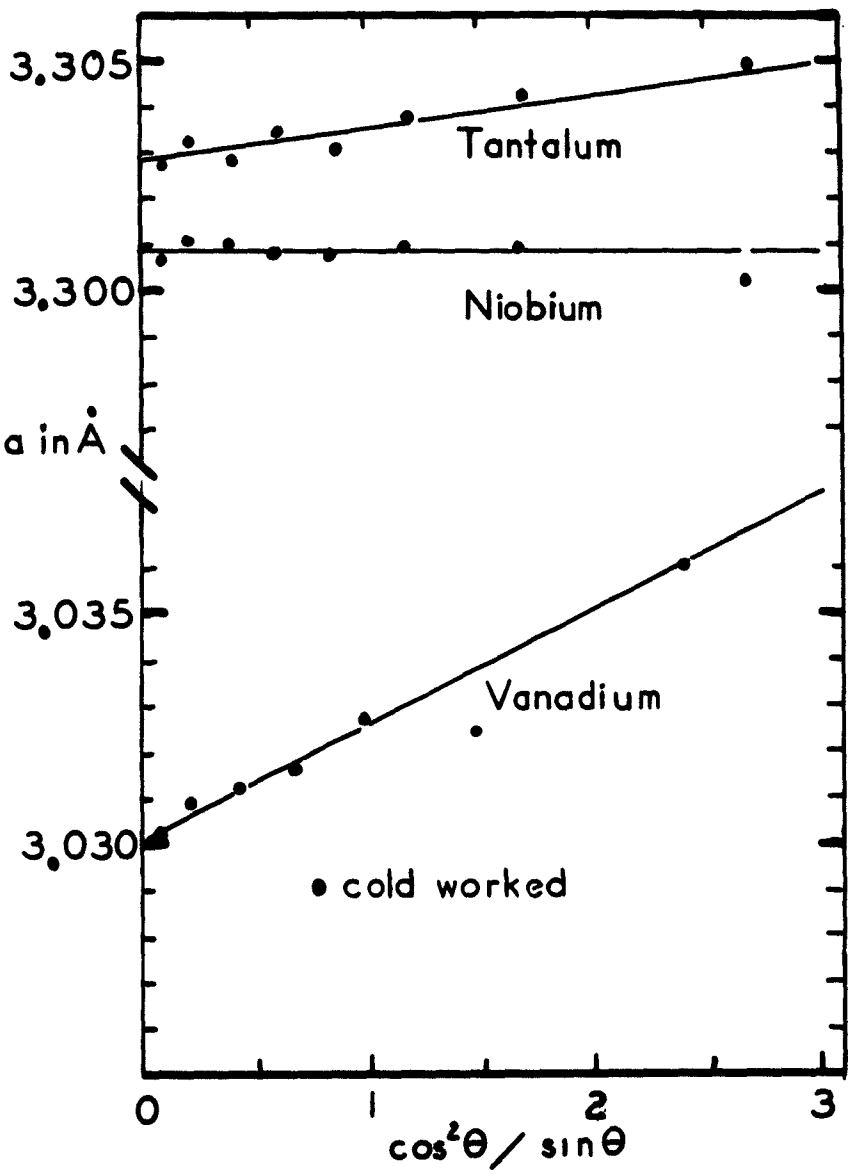
3.305
3.300
3.035
3.030
a in Å
Tantalum
Niobium
Vanadium
• cold worked
0
1
2
3
cos²θ / sinθ

Figure 3 Fourier coefficients for cold worked chromium as a function of the distance variable $L = nd_{hk\ell}$.

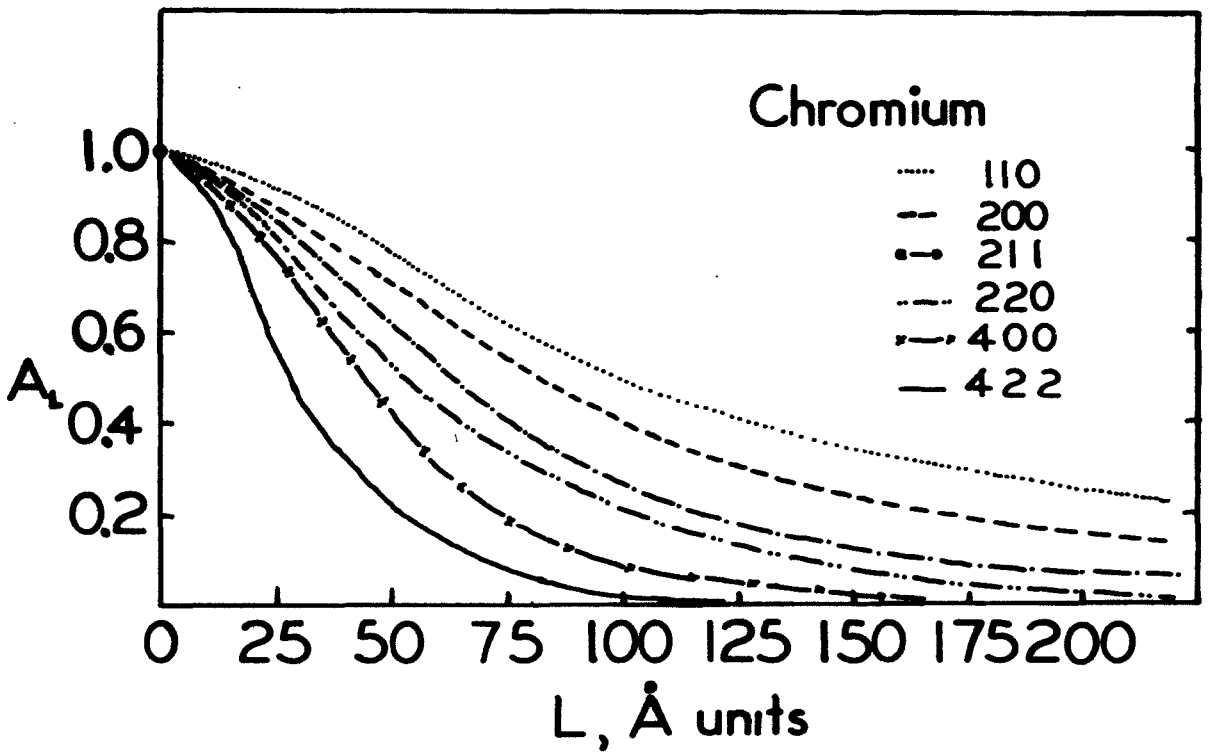
Chromium
110
200
211
220
400
422
1.0
0.8
0.6
0.4
0.2
A_L
0
25
50
75
100
125
150
175
200
L, Å units

Figure 4 Logarithmic representation of Fourier coefficients of chromium as a function of h_o^2, at selected values of L.

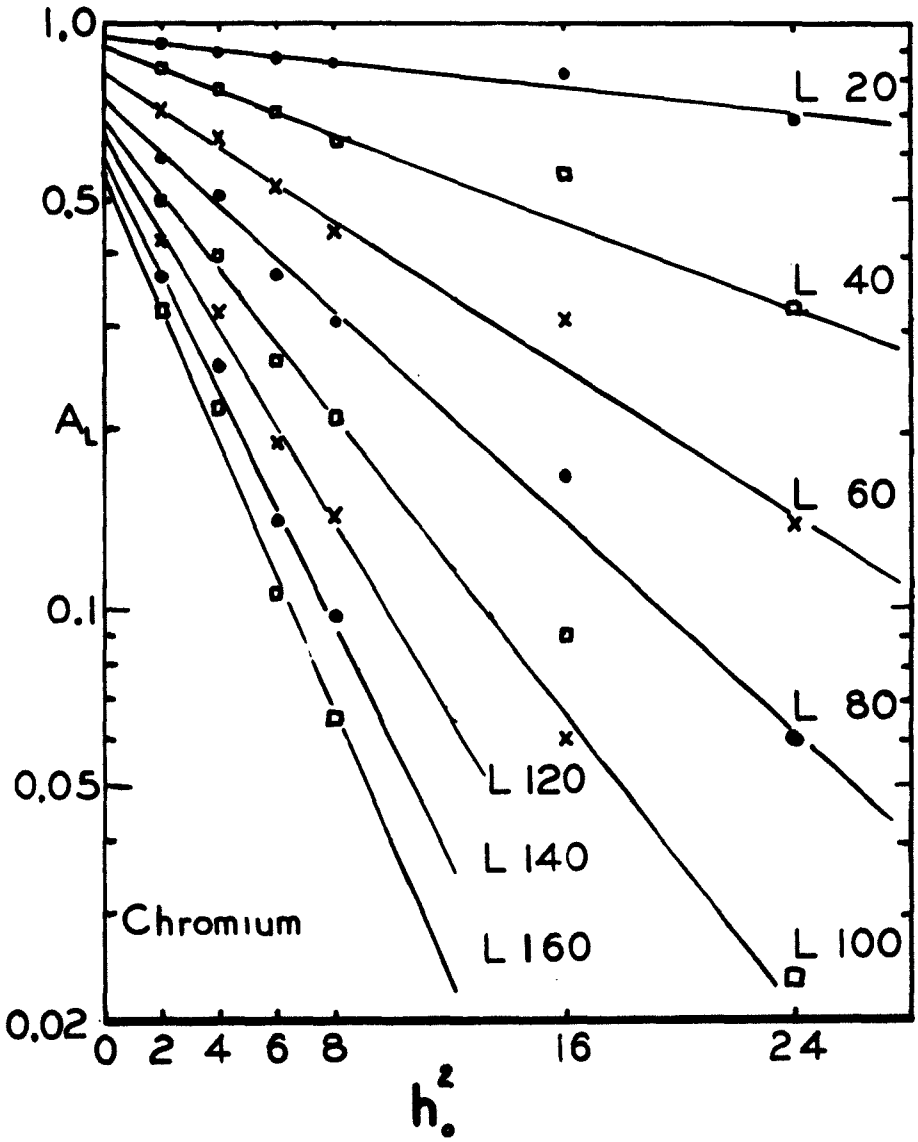
1.0
0.5
A_L
0.1
0.05
0.02
0 2 4 6 8 16 24
h_o^2
L 20
L 40
L 60
L 80
L 100
L 120
L 140
L 160
Chromium

Figure 5 Logarithmic representation of Fourier coefficients of tungsten as a function of h_o^2, at selected values of L.

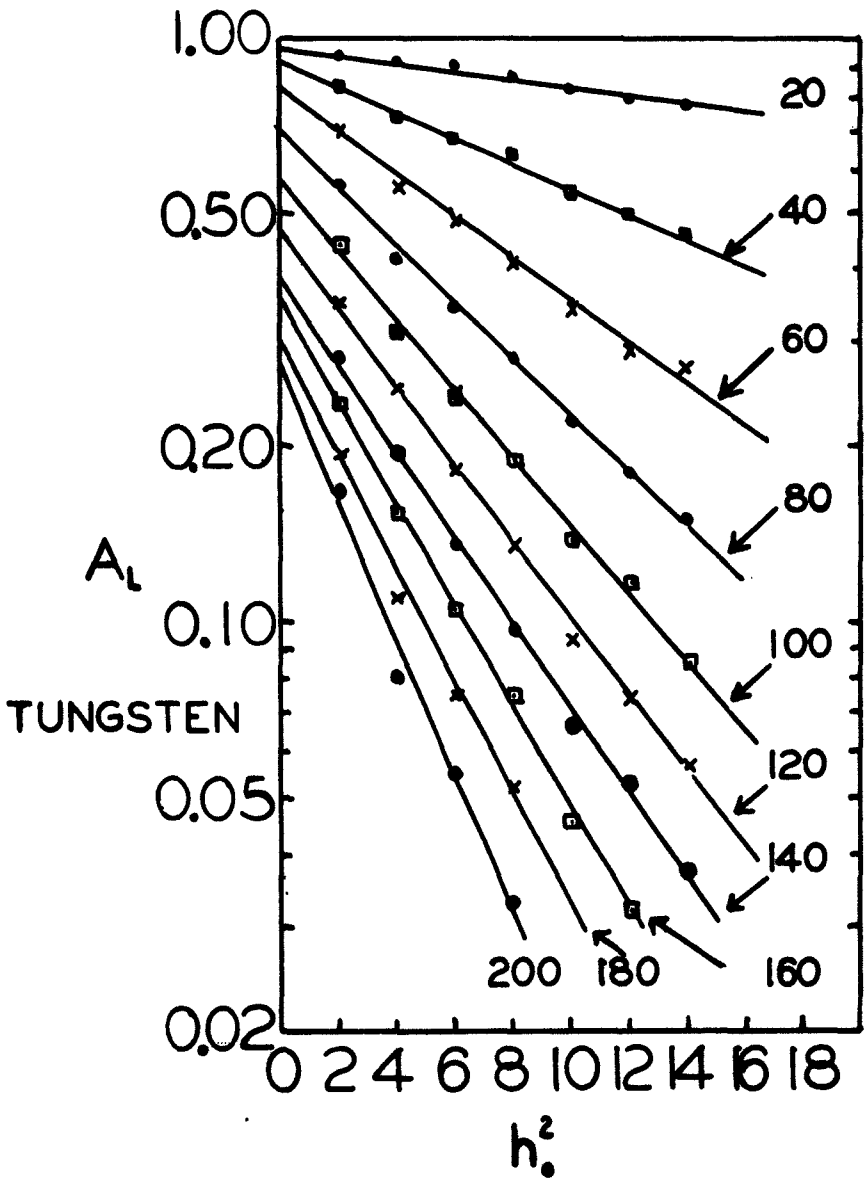
1.00
0.50
0.20
0.10
0.05
0.02
A_L
TUNGSTEN
20
40
60
80
100
120
140
160
180
200
0 2 4 6 8 10 12 14 16 18
h_o^2

Figure 6 Logarithmic representation of Fourier coefficients of vanadium as a function of h_o^2, at selected values of L.

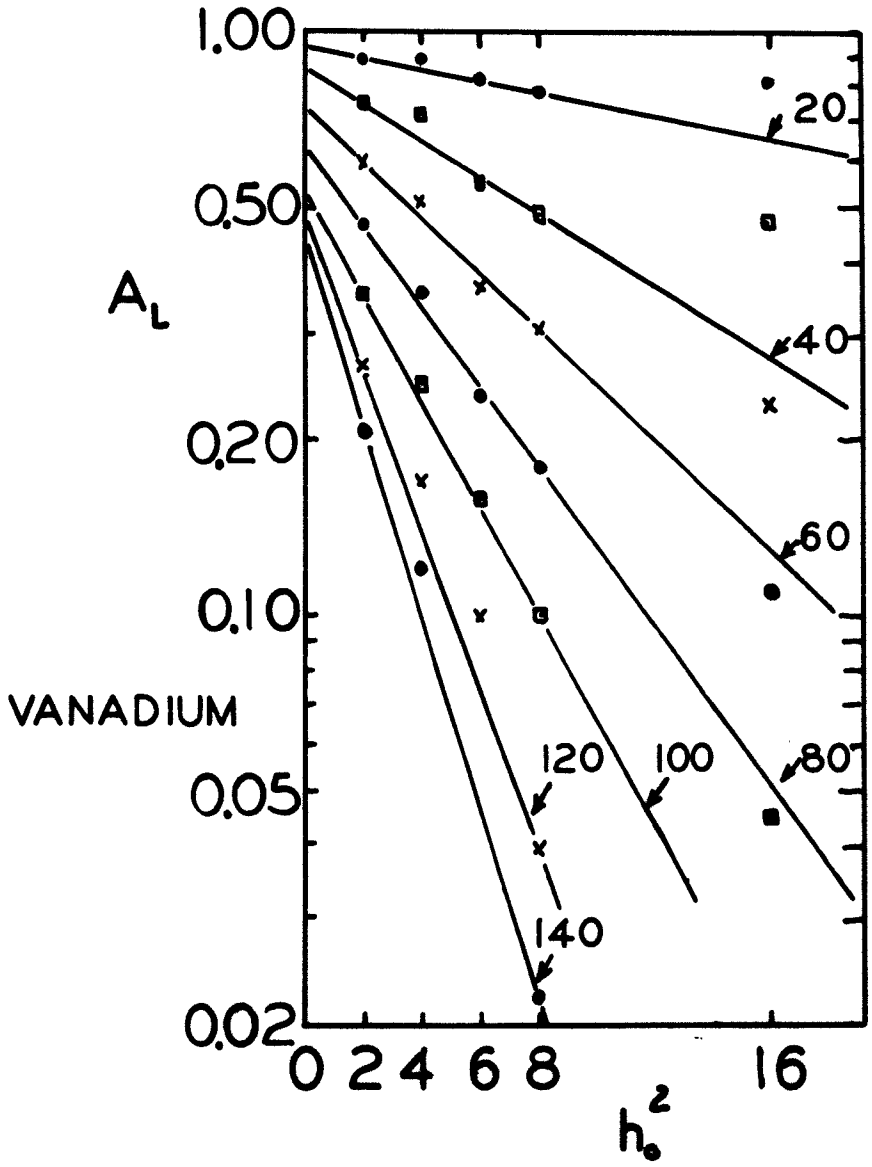
1.00
0.50
0.20
0.10
0.05
0.02
A_L
VANADIUM
20
40
60
80
100
120
140
0 2 4 6 8
16
h_o^2

Figure 7 Logarithmic representation of Fourier coefficients of niobium as a function of h_o^2, at selected values of L.

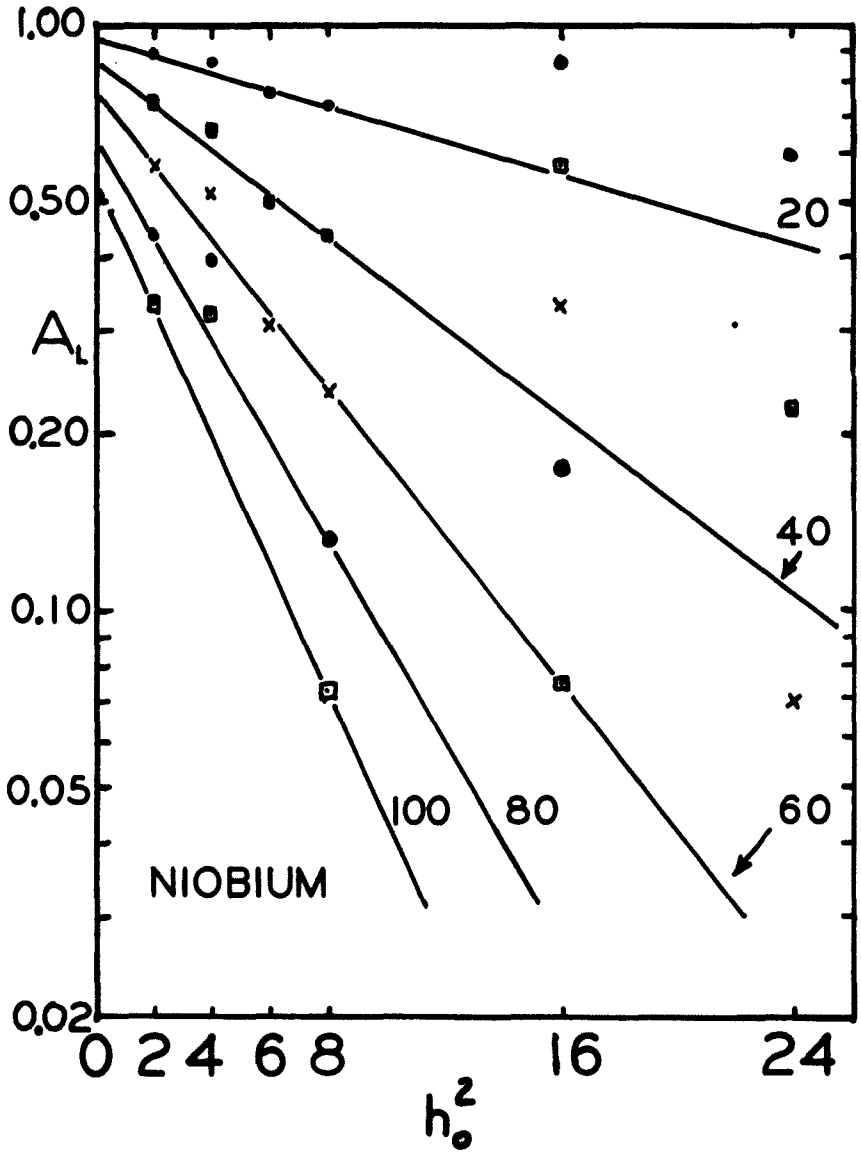
1.00
0.50
0.20
0.10
0.05
0.02
A_L
0 2 4 6 8 16 24
h_o^2
20
40
60
80
100
NIOBIUM

Figure 8 Logarithmic representation of Fourier coefficients of tantalum as a function of h_o^2, at selected values of L.

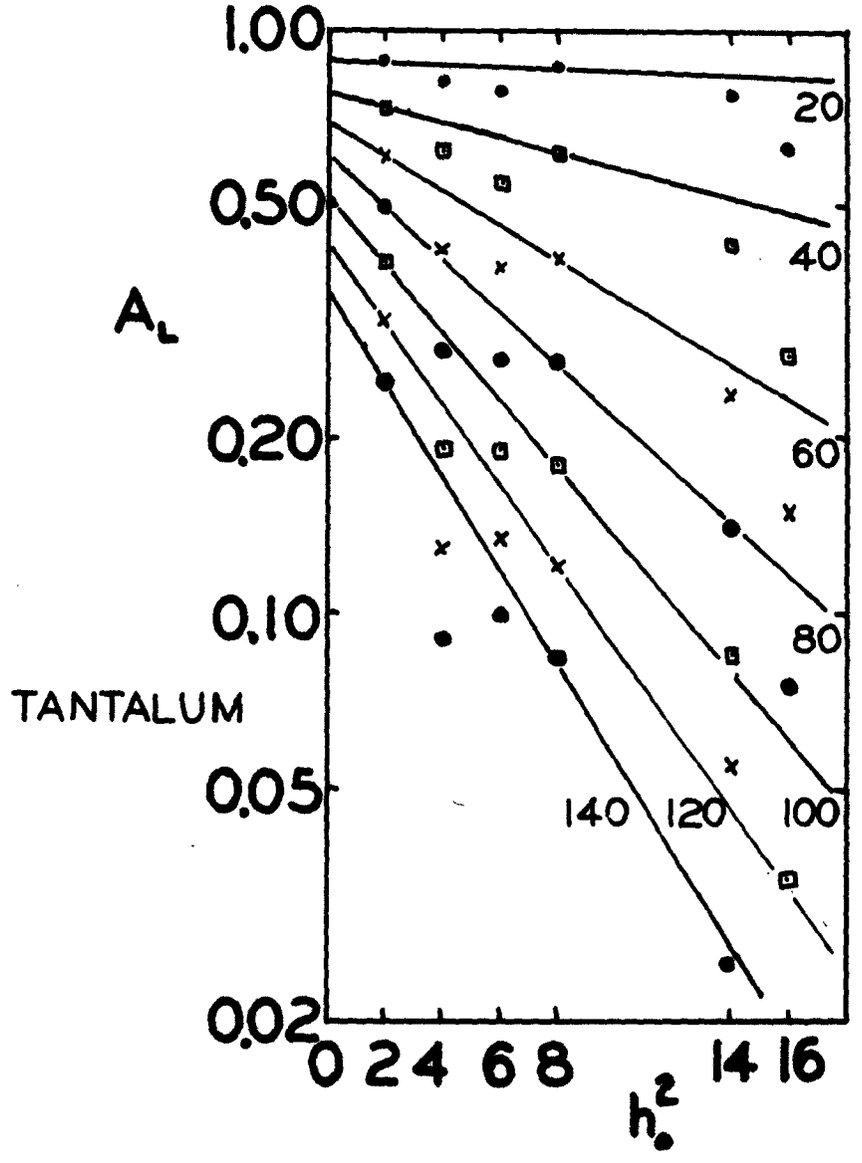
1.00
0.50
0.20
0.10
0.05
0.02
A_L
TANTALUM
20
40
60
80
100
120
140
0 2 4 6 8 14 16
h_o^2

Figure 9 Variation of root mean squared strain as a function of L in different crystallographic directions for tungsten, chromium and vanadium.

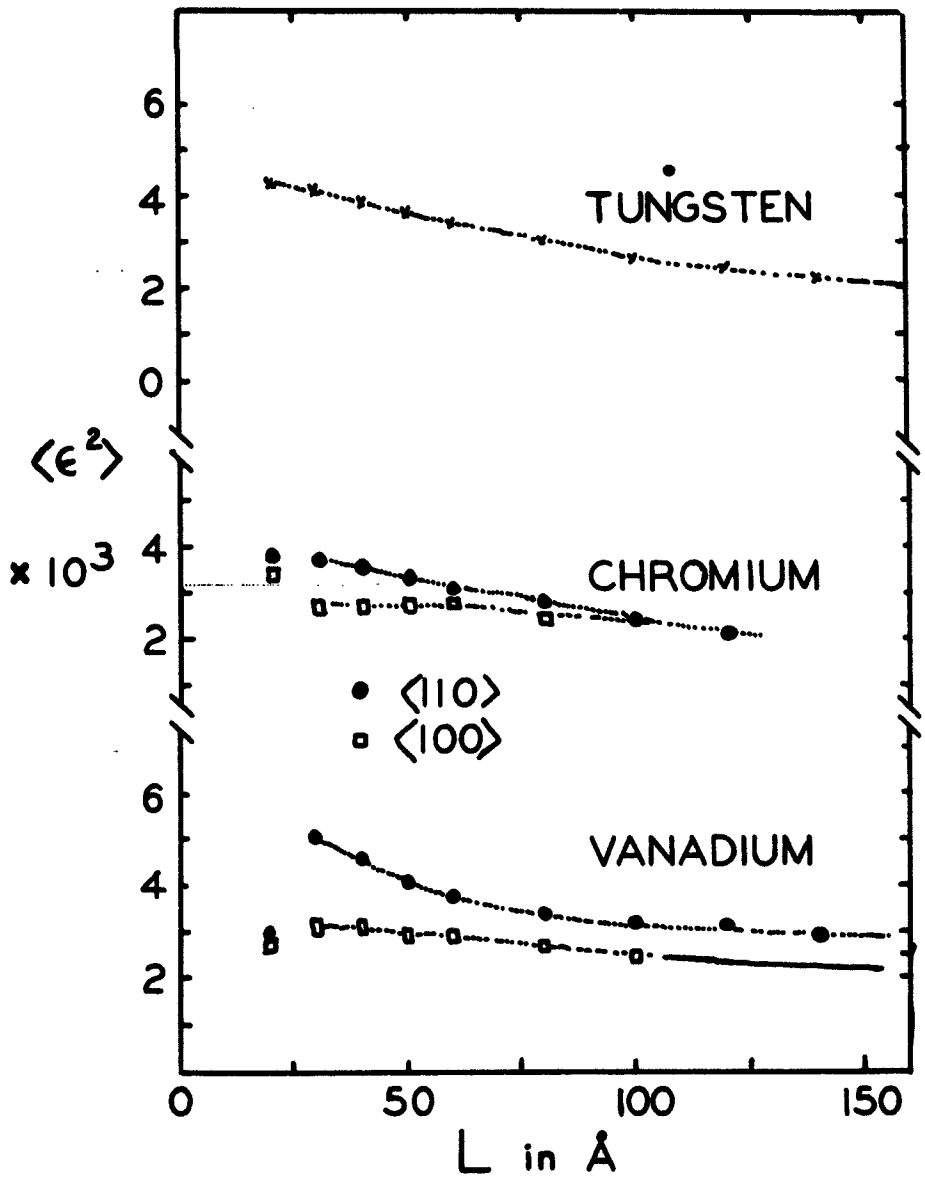
TUNGSTEN
CHROMIUM
VANADIUM
⟨110⟩
⟨100⟩
⟨ε²⟩
x 10³
L in Å
0
50
100
150
6
4
2
0
6
4
2
4
2

Figure 10 Variation of root mean squared strain as a function of L in different crystallographic directions for niobium and tantalum.

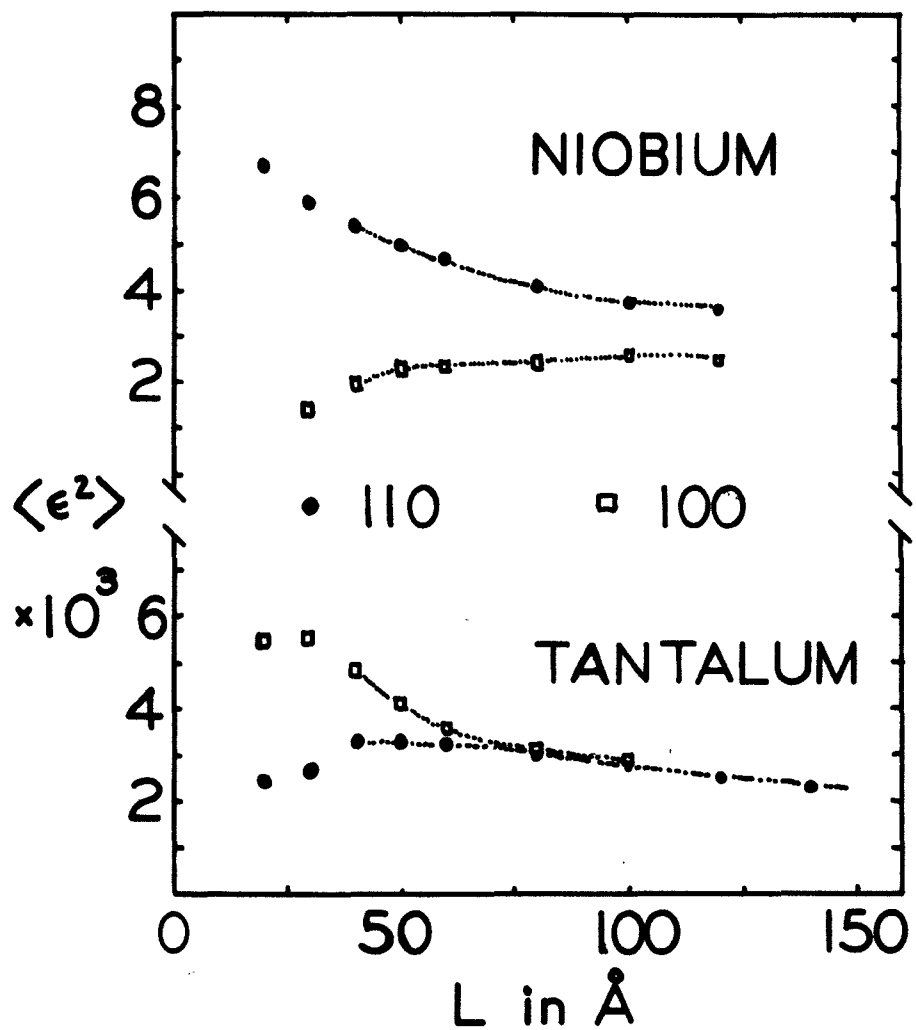
NIOBIUM
TANTALUM
110
100
$\langle \epsilon^2 \rangle$
$\times 10^3$
8
6
4
2
6
4
2
0
50
100
150
L in Å

Figure 11 Variation of the ratio of effective particle sizes and of the ratio of root mean squared strains in the ⟨110⟩ to ⟨100⟩ direction as functions of the elastic anistropy.

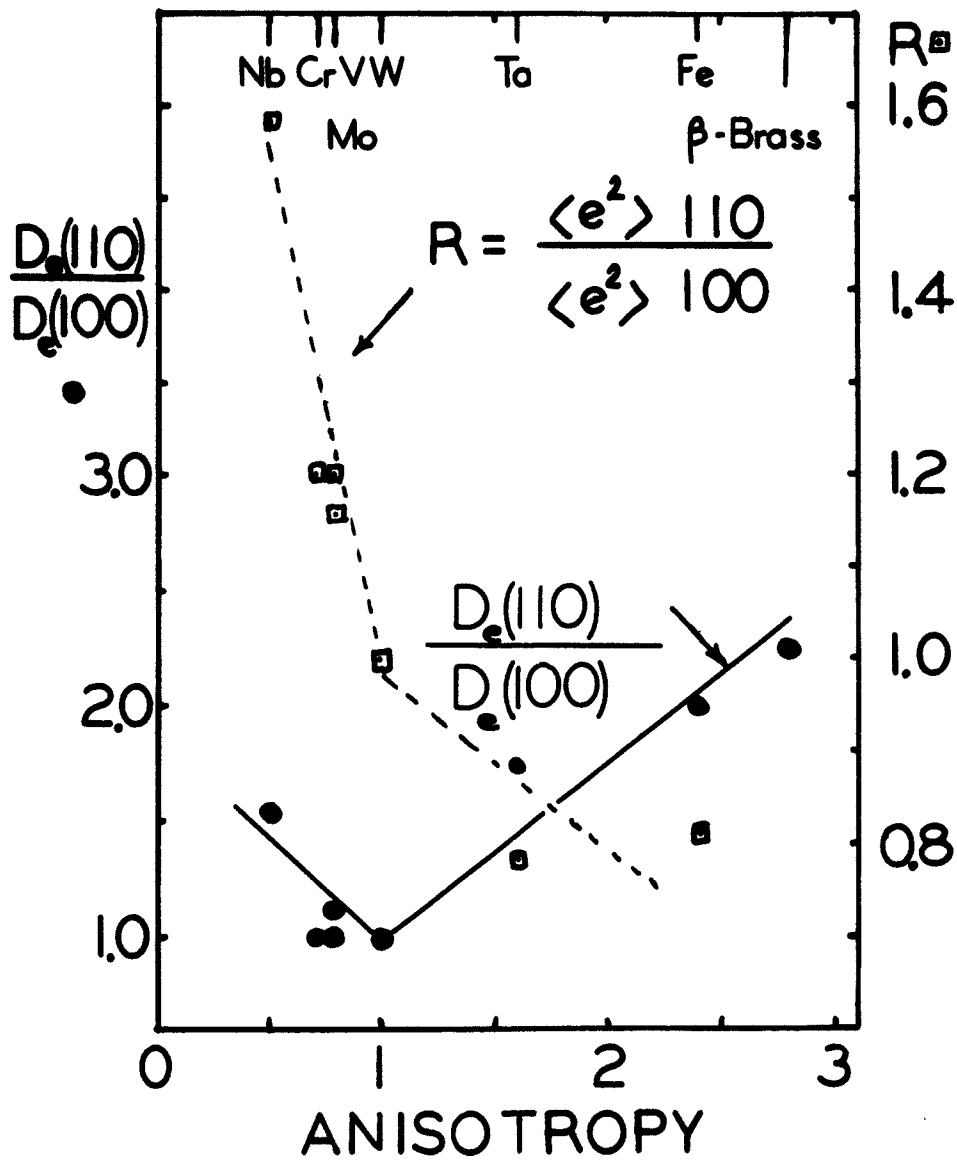
Nb
Cr
V
W
Ta
Fe
Mo
β-Brass
R = ⟨e²⟩ 110 / ⟨e²⟩ 100
D_e(110) / D_e(100)
D_e(110) / D_e(100)
R
3.0
2.0
1.0
1.6
1.4
1.2
1.0
0.8
0
1
2
3
ANISOTROPY